DALTON
FULL PAPER

Structural and electronic variations in cobalt–alkyne clusters †

Tom J. Snaith,[a] Paul J. Low,*[a] Roger Rousseau,[b] Horst Puschmann[a] and Judith A. K. Howard[a]

[a] *Department of Chemistry, University of Durham, South Road, Durham, UK DH1 3LE*
[b] *Steacie Institute for Molecular Sciences, 100 Sussex Drive, Ottawa, Ontario, K1A 0R6, Canada*

Received 19th October 2000, Accepted 23rd November 2000
First published as an Advance Article on the web 15th January 2001

The complexes $[Co_2(\mu\text{-}\eta^2\text{-}HC_2C_6H_4X\text{-}4)(CO)_4(dppm)]$ (X = H, NMe_2, NO_2, CN or C≡C{$Ru(PPh_3)_2Cp$}) and $[Co_2(\mu\text{-}\eta^2\text{-}RC_2C{\equiv}C\{Ru(PPh_3)_2Cp\})(CO)_4(dppm)]$ (R = H or $SiMe_3$) have been prepared and characterised crystallograpically. Electrochemical and spectroscopic evidence has been used to help formulate an empirical MO scheme and thereby explain the nature of the electronic interactions that occur between the pendant group and the Co_2C_2 cluster core.

Introduction

In recent times the search for molecular systems that are able to convey electronic effects between two or more remote sites efficiently has become an area of increasing endeavor, primarily as a result of the interest in the construction of molecular scale electronic devices.[1–5] Electronic interactions between the sites may be manifest in the spectroscopic or electrochemical response of the assembly, and in appropriate cases the mechanism of interaction may be identified, or at least alluded to, by analysis of these parameters.

Interactions between identical mono-nuclear or cluster-based redox active probe groups bridged by ynyl and polyynyl spacers have been studied extensively.[6–12] The $(C{\equiv}C)_n$ π^* orbitals are generally too high in energy to interact significantly with filled metal-based orbitals in the systems examined to date, and classical back-bonding mechanisms are unlikely to play any significant role in the electronic structure of these complexes. Instead, it has been concluded that the strong electronic communication in these systems is a result of efficient mixing between filled metal fragment and polyyne-based orbitals. As a result of these strong orbital interactions the properties of the assembly may differ significantly from those of the individual components.

Several recent studies have identified unusual spectroscopic and electrochemical features associated with complexes which feature two dissimilar redox active fragments linked by (poly)-ynyl bridges and interpreted in terms of varying degrees of electronic "communication" between the fragments.[13–16] In the case of $[Co_2(\mu\text{-}\eta^2\text{-}Me_3SiC_2C{\equiv}CC{\equiv}C\{Ru(PPh_3)_2Cp\})(CO)_4(dppm)]$ and $[Co_2(\mu\text{-}\eta^2\text{-}Me_3SiC{\equiv}CC_2C{\equiv}C\{Ru(PPh_3)_2Cp\})(CO)_4(dppm)]$ electronic interactions between the mononuclear and cluster centres were found to result from strong filled orbital–filled orbital interactions along the length of the $Ru(C{\equiv}C)_nC_2Co_2$ fragment, which gave rise to a delocalised HOMO with significant Ru, C≡C and cluster character, and the dipolar nature of the ground state.[17] Now, in order to explore further the role played by the bridge in these systems, we have examined the structural, electrochemical and spectroscopic properties of a series of compounds $[Co_2(\mu\text{-}\eta^2\text{-}HC_2C_6H_4X\text{-}4)(CO)_4(dppm)]$ (X = H, NMe_2, NO_2, CN or C≡C[$Ru(PPh_3)_2Cp$]) and compared them with the simple alkynyl complexes $[Co_2(\mu\text{-}\eta^2\text{-}RC_2C{\equiv}C\{Ru(PPh_3)_2Cp\})(CO)_4(dppm)]$ (R = H or $SiMe_3$).

† Dedicated to the memory of Ron Snaith, a much loved product of this Department and father to Tom.

Results

Synthesis

The series of complexes $[Co_2(\mu\text{-}\eta^2\text{-}HC_2C_6H_4X\text{-}4)(CO)_4(dppm)]$ were prepared by reaction of the appropriately substituted phenyl acetylene $HC_2C_6H_4X$-4 with $[Co_2(CO)_6(dppm)]$ (X = H, 56%, **1**; NMe_2, 61%, **2**; NO_2, 59%, **3**; CN, 89%, **4**).[18] The NMR data for these complexes were unremarkable (Table 1). The cluster bound proton Co_2C_2H was found as a triplet (J_{HP} = 7–8 Hz) near δ 5.8, the precise position of which showed some dependence on the electronic nature of the X group (**1**, 5.78; **2**, 5.72; **3**, 5.84; **4**, 5.83). The positive and negative ion electrospray mass spectra (ES MS) collected in methanolic solutions containing a small amount of NaOMe were characterised by highest molecular weight ions corresponding to $[M + Na]^+$ and $[M - H]^-$ respectively.[19]

The metal acetylide substituted analogue $[Co_2(\mu\text{-}\eta^2\text{-}Me_3Si\text{-}C_2C_6H_4C{\equiv}C\{Ru(PPh_3)_2Cp\})(CO)_4(dppm)]$ **5** was prepared from the reaction of $[Ru(C{\equiv}CC_6H_4C{\equiv}CSiMe_3)(PPh_3)_2Cp]$ with $[Co_2(CO)_6(dppm)]$ in benzene, and isolated as a tan coloured crystalline solid in good yield. The NMR spectra were characterised by the resonances expected for the $SiMe_3$ and Cp ligands and the ^{13}C resonances of the cluster core and alkynyl carbon centres, which have been assigned on the basis of the magnitude of the J_{CP} coupling constants (Table 1). The positive and negative ion mass spectra of **5** are characterised by $[M + Na]^+$ and $[M - H]^-$ ions, respectively.

Complexes in which the cobalt–carbon carbonyl cluster was attached directly to a pendant metal acetylide moiety were readily prepared from the cluster substituted terminal alkynes $[Co_2(\mu\text{-}\eta^2\text{-}RC_2C{\equiv}CH)(CO)_4(dppm)]$ (R = $SiMe_3$ **7** or H, **8**). Treatment of **7** or **8** with one equivalent of $[RuCl(PPh_3)_2Cp]$ in the presence of NH_4PF_6 in methanol afforded the vinylidene complex $[Ru\{{=}C{=}C(H)[C_2Co_2(R)(CO)_4(dppm)]\}(PPh_3)_2Cp]PF_6$ which was not isolated but rather deprotonated *in situ* by addition of a methanolic solution of sodium methoxide to afford the strikingly green complexes $[Co_2(\mu\text{-}\eta^2\text{-}RC_2C{\equiv}C\{Ru\text{-}(PPh_3)_2Cp\})(CO)_4(\mu\text{-}dppm)]$ (R = $SiMe_3$ **9** or H, **10**) (Table 1). For **9**, the ^1H and ^{13}C NMR spectra contained the anticipated resonances of the $SiMe_3$ and Cp ligands, while a triplet resonance at δ_C 36.88 (J_{CP} = 20 Hz) was readily assigned to the methylene carbon of the dppm ligand. The quaternary carbons of the alkynyl bridge and Co_2C_2 cluster core were not observed. The ES MS of **9** obtained from solutions containing a small amount of NaOMe as an *in situ* aid to chemical ionisation afforded the ions $[M + Na]^+$, $[M]^+$ and a fragment ion derived

 DOI: 10.1039/b008445j

Table 1 Spectroscopic data for complexes **1**–**5**, **9**, **10**

Complex	Colour	Yield (%)	$\tilde{\nu}$(CO)[a]/cm^{-1}	Analysis (%)[b]			ES MS[c] *m*/*z*	δ(*J*/Hz)	
				C	H	N		^{1}H NMR[e]	^{13}C NMR[e]
1	Red	56	2027vs, 1999s, 1975s, 1956w	62.56 (62.03)	4.28 (3.94)		ES(+): 739, $[M + Na]^+$; 711, $[M + Na - CO]^+$; 688, $[M - CO]^+$ ES(−): 715, $[M - H]^-$; 687, $[M - H - CO]^-$	3.10 (dt, 1H, J_{HP} = 13, J_{HH} = 10, CHP_2); 3.61 (dt, 1H, J_{HP} = 13, J_{HH} = 10, CHP_2); 5.78 (t, 1H, J_{HP} = 7, Co_2C_2H); 7.20–7.67 (m, 25H, Ph)	41.23 (t, J_{CP} = 21, CH_2P_2); 96.30 [t, J_{CP} = 16, C(3/4)]; 126.09–142.87 (m, Ph); 203.00, 207.04 (2 × br, CO)
2	Purple	61	2023vs, 1995s, 1971vs, 1952w	61.55 (61.88)	4.39 (4.38)	1.67 (1.84)	ES(+): 782, $[M + Na]^+$; 759, $[M]^+$; 731, $[M - CO]^+$ ES(−): 758, $[M - H]^-$; 730, $[M - H - CO]^-$	2.98 (m, 6H, 2 × Me); 3.05 (dt, 1H, J_{HP} = 13, J_{HH} = 10, CHP_2); 3.55 (dt, 1H, J_{HP} = 13, J_{HH} = 10, CHP_2); 5.72 (t, 1H, J_{HP} = 8, Co_2C_2H); 6.70–7.58 (m, 24H, Ph)	72.64 [s, C(3/4)]; 97.98 [t, J_{CP} = 16, C(3/4)]; 112.20 [s, C(31)]; 128.17 – 149.22 (m, Ph); 203.34, 207.63 (2 × br, 2 × CO)
3	Dark red	59	2030s, 2003vs, 1970s, 1963w	57.80 (58.36)	3.57 (3.57)	1.78 (1.84)	ES(+): 784, $[M + Na]^+$ ES(−): 760, $[M - H]^-$; 732–704, $[M - H - nCO]^-$ (n = 1 or 2)	3.15 (dt, 1H, J_{HP} = 12, J_{HH} = 10, $PCHP_2$); 3.68 (dt, 1H, J_{HP} = 12, J_{HH} = 10, $PCHP_2$); 5.84 (t, 1H, J_{HP} = 8, Co_2C_2H), 7.23–8.15 (m, 24H, Ph)	41.75 (t, J_{CP} = 21, CH_2P_2); 74.21 [t, J_{CP} = 8, C(3/4)]; 91.78 [t, J_{CP} =16, C(3/4)]; 123.73, [s, C(31)]; 128.30–152.37 (m, Ph); 202.18, 206.33 (2 × br, 2 × CO)
4	Purple	89	2030s, 2006sh, 2002vs, 1978s, 1961w	61.30 (61.54)	3.62 (3.64)	1.84 (1.89)	ES(+): 795, $[M + Na + NCMe]^+$, 764, $[M + Na]^+$	3.14 (dt, 1H, J_{HP} = 12, J_{HH} = 10, CHP_2); 3.67 (dt, 1H, J_{HP} = 12, J_{HH} = 10, CHP_2); 5.83 (t, 1H, J_{HP} = 7, Co_2C_2H); 7.21–1.69 (m, 24H, Ph)	41.60 (t, J_{CP} = 21, CH_2P_2); 73.93 [t, J_{CP} = 8, C(3/4)]; 92.43 [t, J_{CP} = 17, C(3/4)]; 108.47 [s, CN)]; 119.78 [s, C(31)]; 128.22–152.37 (m, 24H. Ph); 202.29, 206.76 (2 × br, 2 × CO)
5	Tan	60	(2075w, br), 2019s, 1993vs, 1968s, 1948w	66.19 (66.36)	4.71 (4.70)		ES(+): 1525, $[M + Na]^+$ ES(−): 1501, $[M - H]^-$	0.35 (s, 9H, $SiMe_3$); 3.22 (dt, J_{HP} = 13, J_{HH} = 11, CHP_2); 3.46 (dt, J_{HP} = 13, J_{HH} = 11, CHP_2); 4.33 (s, 5H, Cp); 6.93–7.52 (m, 54H, Ph)	0.89 (s, $SiMe_3$); 35.61 (t, J_{CP} = 21, CH_2P_2); 85.27 (s, Cp); 88.04 [t, J_{CP} = 10, C(4)]; 107.23 [t, J_{CP} = 8, C(2)]; 115.20 (s, C(3); 116.68 [t, J_{CP} = 23, C(1)]; 127.49–139.62 (m, Ph); 203.36, 207.78 (2 × br, CO)
9	Dark green	51	(2028w), 2004s, 1984vs, 1957s, 1941w	64.75 (64.85)	4.57 (4.66)		ES(+): 1449, $[M + Na]^+$; 1426, $[M]^+$; 1398, $[M - CO]^+$ ES(−): 1425, $[M - H]^-$	0.29 (s, 9H, $SiMe_3$); 3.36 (dt, 1H, J_{HP} = 12, J_{HH} = 10, CHP_2); 3.65 (dt, 1H, J_{HP} = 12, J_{HH} = 10, CHP_2); 4.23 (s, 5H, Cp); 6.78–7.43 (m, 50H, Ph)	1.46 (s, $SiMe_3$); 36.88 (t, J_{CP} = 20, CH_2P_2); 86.24 (s, Cp); 112.29 [s, C(1/2)]; 127.19–139.18 (m, Ph); 206.51, 207.17 (2 × br, CO)
10	Dark green	58	2030s, 2004w, 1981vs, 1954s	[d]			ES(+): 1377, $[M + Na]^+$; 1349, $[M + Na - CO]^+$ ES(−): 1353, $[M - H]^-$	3.20 (br, 1H, CHP_2), 3.45 (br, 1H, CHP_2); 4.28 (s, 5H, Cp); 5.63 (s, 1H, Co_2C_2H); 7.11–7.51 (m, 50H, Ph)	39.95 (t, J_{CP} = 18, CH_2P_2); 86.00 (s, Cp); 112.85 [s, C(1/2)]; 127.46–139.05 (m, Ph); 204.81, 208.42 (2 × br, CO)

[a] In cyclohexane, ν(C≡C) given in parentheses. [b] Required values given in parentheses. [c] In MeOH containing NaOMe. [d] Despite repeated attempts, an accurate microanalysis could not be obtained. [e] In $CDCl_3$ and labelled in accord with the corresponding ORTEP figure.

Table 2 Selected bond lengths (Å) and angles (°) for complexes **1**–**5**, **9**, **11**

	1	**2**	**3**	**4**	**5**	**9**	**11**[a]
Ru–C(1)					2.003(2)	2.012(2)	1.994(5)
Ru–P(3)					2.2849(7)	2.2853(6)	2.297(2)
Ru–P(4)					2.3021(7)	2.2935(6)	2.301(2)
C(1)–C(2)					1.218(4)	1.223(3)	1.202(8)
C(2)–C(3)					1.432(3)[b]	1.410(3)	1.432(7)
C(3)–C(34)	1.468(2)	1.465(3)	1.458(3)	1.463(2)	1.465(3)		
C(3)–C(4)	1.348(2)	1.350(3)	1.356(3)	1.351(3)	1.359(3)	1.368(3)	
Co(1)–Co(2)	2.4875(3)	2.4657(4)	2.4950(4)	2.4707(3)[c]	2.5116(5)	2.4947(4)	
Co(1)–C(3)	1.9727(15)	1.9857(19)	1.9591(14)	1.9516(14)	1.948(2)	1.972(2)	
Co(1)–C(4)	1.9508(16)	1.9577(19)	1.9609(14)	1.9662(15)	1.997(3)	1.981(2)	
Co(2)–C(3)	1.9470(15)	1.9434(19)	1.9591(14)	1.9516(14)[c]	1.981(2)	1.990(2)	
Co(2)–C(4)	1.9660(16)	1.9674(19)	1.9609(14)	1.9662(15)[c]	1.971(2)	1.986(2)	
C(31)–C(32)	1.391(3)	1.410(3)	1.394(3)	1.392(3)	1.411(3)		1.41(1)
C(32)–C(33)	1.390(2)	1.391(3)	1.387(3)	1.392(3)	1.383(3)		1.370(7)
C(33)–C(34)	1.403(2)	1.402(3)	1.412(3)	1.405(3)	1.408(3)		1.363(8)
C(34)–C(35)	1.401(2)	1.404(3)	1.406(3)	1.402(3)	1.400(3)		1.37(1)
C(35)–C(36)	1.395(2)	1.384(3)	1.392(3)	1.386(3)	1.387(3)		1.373(8)
C(36)–C(31)	1.388(3)	1.409(3)	1.387(3)	1.397(3)	1.410(4)		1.400(8)
Ru–C(1)–C(2)					171.7(2)	166.61(18)	175.9(4)
C(1)–C(2)–C(3)					174.6(3)[b]	177.6(2)	175.0(9)
C(2)–C(3)–C(4)	142.60(15)[d]	143.41(18)[d]	141.81(17)[d]	144.82(17)[d]	138.2(2)[b]	144.7(2)	

[a] From ref. 14. [b] Read C(31) for C(3). [c] Read Co(1)#1 for Co(2). [d] Read C(34) for C(2).

from the loss of a carbonyl ligand $[M - CO]^+$. The negative ion spectrum of the same solution contained the $[M - H]^-$ ion at *m*/*z* 1425. Metallation of **8** by the $Ru(PPh_3)_2Cp$ fragment occurred only at the terminal acetylenic position as indicated by NMR data, with Co_2C_2H and Cp resonances being detected along with those of the dppm ligand. Again, the quaternary carbons could not be identified. The positive and negative ion ES MS of **10** contained $[M + Na - nCO]^+$ ($n = 0$ or 1) and $[M - H]^-$ ions, respectively.

Molecular structures

Single-crystal X-ray diffraction studies were performed on complexes **1**–**5** and **9**. Important bond lengths and angles are summarised in Table 2. These structural studies serve the obvious purpose of confirming the structures and highlight the role of steric influences on the overall molecular shape. As the primary interest in these complexes lies in the exploration of electronic interactions between the various fragments, it is tempting to search the metrical parameters carefully for evidence of structural distortion, particularly in the M–C, C≡C and C–C_2Co_2 bond lengths. However, the structural perturbations associated with these fragments in different electronic environments are subtle and such differences as there are often fall within the range of the experimental errors.[20] Suffice to say any conclusions based solely on very small differences in structure must be made with caution.

$[Co_2(\mu\text{-}\eta^2\text{-}HC_2C_6H_4X\text{-}4)(CO)_4(\mu\text{-dppm})]$ (X = H, 1; NMe_2, 2; NO_2, 3 or CN, 4). The molecular structures of the phenyl substituted Co_2C_2 clusters **1**–**4** are illustrated in Figs. 1–4. The dppm ligand occupies an *exo* position relative to the pendant phenyl ring, in response to steric demands. Across the series, and within experimental error, the C(3)–C(4) bond length is invariant (Table 2). The Co(1)–Co(2) separations range from 2.4657(4) (X = *p*-NMe_2, **2**) to 2.4950(4) Å (X = *p*-NO_2, **3**). Remaining cluster parameters including Co(1,2)–C(3,4) are comparable across the series and show no clear variation with the electronic nature of the phenyl substituent. Most of the differences in C–C bond lengths within the C(31)–(36) phenyl ring are within the 3σ level of confidence, although C(32,35)–C(33,36) appear to be relatively short (Table 2).

Perhaps the most significant aspect of the structural determination is the orientation adopted by the phenyl ring

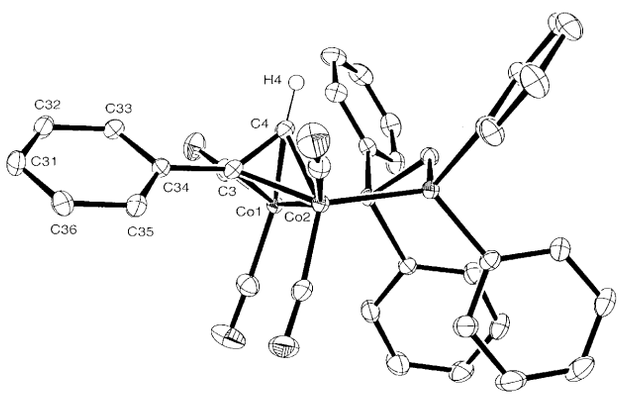

Fig. 1 Molecular structure of complex **1** showing the atom labelling scheme. Phenyl hydrogen atoms are omitted.

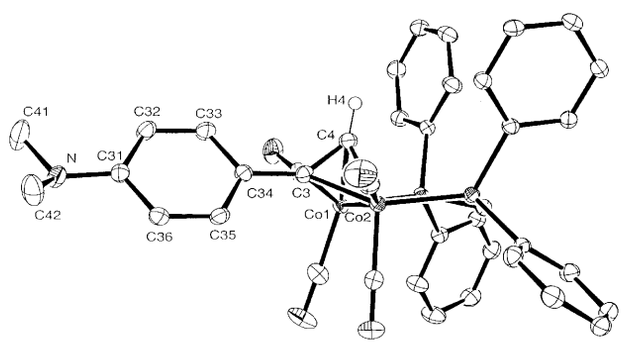

Fig. 2 Molecular structure of complex **2**. Details as in Fig. 1.

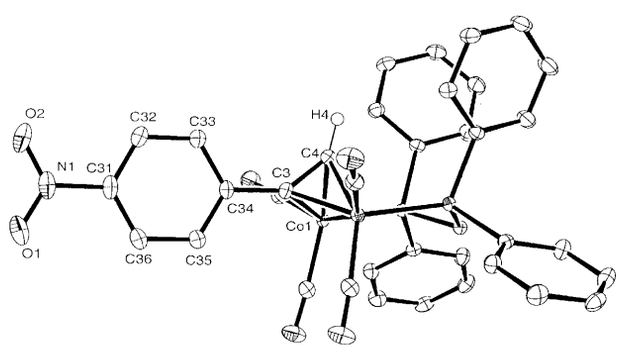

Fig. 3 Molecular structure of complex **3**. Details as in Fig. 1.

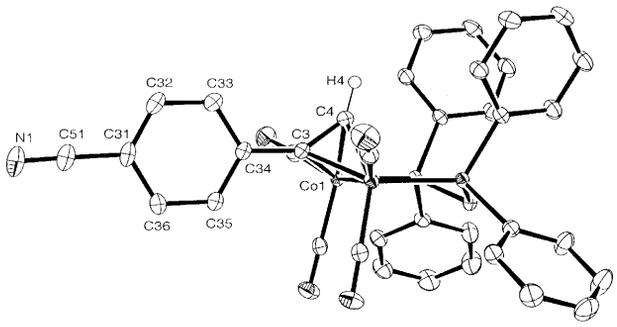

Fig. 4 Molecular structure of complex **4**. Details as in Fig. 1.

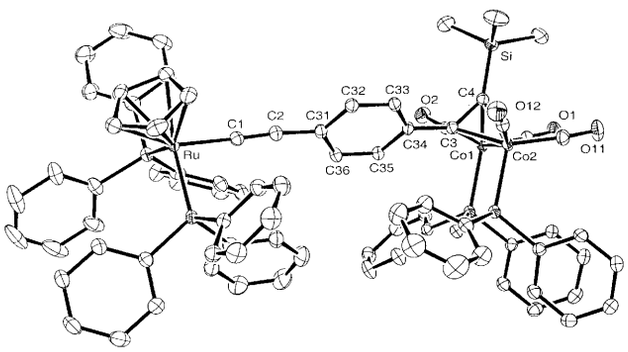

Fig. 5 Molecular structure of complex **5**. Details as in Fig. 1.

relative to the plane normal to the Co–Co vector. In the case of complexes **1** and **2** the C(4)–C(3)–C(34)–C(33) torsion angles are 46.2 and 29.5°, respectively. For **3** and **4** which feature the electron-withdrawing NO_2 and CN groups the phenyl ring lies in the crystallographic mirror plane and the C(4)–C(3)–C(34)–C(33) torsion angle is therefore 180° in both cases. There are no obvious close intermolecular separations within the unit cells of **1**–**4** and given the correlation with the electronic properties of the substituent it appears unwise to attribute categorically this variation in orientation of the phenyl ring simply to crystal packing forces. We defer further comment on this point to the Discussion (see below).

$[Co_2(\mu\text{-}\eta^2\text{-}Me_3SiC_2C_6H_4C{\equiv}C\{Ru(PPh_3)_2Cp\})(CO)_4(\mu\text{-dppm})]$ 5. The structure of compound **5** is shown in Fig. 5. It clearly shows a mononuclear half-sandwich cyclopentadienyl bis(triphenylphosphine) ruthenium fragment attached to the Co_2C_2 tetrahedron *via* a phenylacetylide bridge. The conformation adopted is that which minimises the steric interactions between the dppm ligand and trimethylsilyl group. The cluster core parameters are consistent with those of **1** and **2**, although twisting of the C(3)–C(4) vector relative to the Co–Co bond makes direct comparison of the metrical parameters difficult. Theoretical analysis of dicobalt alkyne complexes suggests that the orientation of the alkyne bond relative to the Co–Co vector is sensitive to electronic effects,[21] and pronounced rotation of the alkyne vector has been observed following oxidation of $[Co_2(\mu\text{-}\eta^2\text{-}MeC_2Me)(CO)_2(dppm)_2]$.[22]

The Ru–P(3,4) and C(1)–C(2) bond lengths found in complex **5** are in better agreement with the analogous bonds in $[Ru(C{\equiv}C\text{-}C_6H_4NO_2\text{-}4)(PPh_3)_2Cp]$ **11**[23] (Table 2) than $[Ru(C{\equiv}CC_6H_5)(PPh_3)_2Cp]$.[24] However, the C(32)–C(33) [1.383(3) Å] and C(35)–C(36) [1.387(3) Å] separations are shorter than C(31)–C(32,36) [1.411(3); 1.410(4) Å] and C(34)–C(33,35) [1.408(3); 1.400(3) Å]. Bond length alternation is not apparent in **11**. The plane of the phenyl ring in **5** bisects the P(1)–Ru–P(2) bond angle and lies in the pseudo mirror plane of the ruthenium fragment. The C(4)–C(3)–C(34)–C(33) torsion angle is of comparable magnitude, but opposite sign (−48.4°), to that found for **1**.

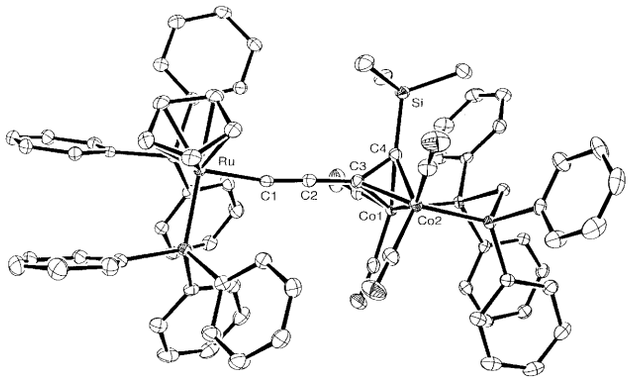

Fig. 6 Molecular structure of complex **9**. Details as in Fig. 1.

$[Co_2(\mu\text{-}\eta^2\text{-}Me_3SiC_2C{\equiv}C\{Ru(PPh_3)_2Cp\})(CO)_4(\mu\text{-dppm})]$ 9. An ORTEP projection of complex **9** is shown in Fig. 6 and selected bond lengths and angles are given in Table 2. The dppm ligand spans the Co(1)–Co(2) vector occupying coordination sites approximately *trans* to the C(1) and C(2) atoms of the bridge. This presumably arises from the steric constraints imposed by the bulky triphenylphosphine ligands of the ruthenium fragment which force the dppm ligand to occupy a site closer to the bulky trimethylsilyl group capping the cluster than might otherwise be expected. Further to relieve steric interactions between the Cp, PPh_3 and cluster bound $SiMe_3$ ligands, the Ru–C(1)–C(2) bond angle is distorted from linearity [166.6(2)°]. The P(3)–Ru–P(4) bond angle [100.78(2)°] is somewhat smaller than in the case of **11**. Other bonding parameters of the mononuclear ruthenium fragment are comparable with those of **11** with the average Ru–Cp (2.240 Å), Ru–C(1) [2.012(2) Å] and Ru–P bond lengths being equivalent within experimental error. The C(2)–C(3) bond length [1.410(3) Å] is the same as the analogous bond in $[Co_2(\mu\text{-}\eta^2\text{-}(Me_3SiC{\equiv}CC_2C{\equiv}C\{Ru(PPh_3)_2Cp\})(CO)_4(dppm)]$ [1.407(3) Å].[17] Similarly, there are no significant deviations in the bond lengths of **9** when compared with those of the analogous compound $[Co_2(\mu\text{-}\eta^2\text{-}HC_2C{\equiv}C\{Ru(PPh_3)_2Cp\})(CO)_4(\mu\text{-dppm})]$ **10**,[25] although the relatively low quality of the data obtained in the latter case precludes detailed comparisons. The elongation of the Co(1)–C(3), Co(2)–C(4) bonds and contraction of Co(1)–C(4), Co(2)–C(3) bonds in **5** relative to **9** is consistent with the small twist in the direction of the Co(1)–Co(2) vector relative to that of C(3)–C(4) (89.6, **9**; 91.9°, **5**).

Electrochemistry

The phenyl-substituted cluster **1** displayed two redox waves, the reversibility of which improved at sub-ambient temperatures. At −30 °C a fully chemically reversible reduction and an oxidation process which was only partially chemically reversible were observed (Table 3). Complex **2** displayed well behaved electrochemical behaviour at room temperature and the cyclic voltammogram displayed two closely spaced oxidation waves and a single reversible reduction process. In contrast, the NO_2 analogue **3** displays a single oxidation wave and two reduction waves. The reduction of **3** to $\mathbf{3}^{\bullet-}$ was found to be reversible when examined in isolation and on the basis of the trends in E° found throughout this series of compounds is assigned to the Co_2C_2 core. The second totally irreversible reduction at −1.49 V is assigned to the $C_6H_4NO_2$-4 moiety. The CV of **5** appears grossly similar to that of **2** and involves a single reversible one-electron reduction and two one-electron oxidation processes. Studies of the first oxidation process in isolation revealed it to be fully reversible.

Compounds $[Co_2(\mu\text{-}\eta^2\text{-}Me_3SiC_2C{\equiv}CSiMe_3)(CO)_4(dppm)]$ **6**, **7** and **8** form a structurally similar series containing a single Co_2C_2 redox-active site bearing a pendant acetylide ligand.

Table 3 Electrochemical data for complexes **1**–**3** and **5**–**10**[a]

Complex	E°_{Ox1}/V ($i_{pa}:i_{pc}$) [ΔE_p]/V	E°_{Ox2}/V ($i_{pa}:i_{pc}$) [ΔE_p]/V	E°_{Red1}/V ($i_{pa}:i_{pc}$) [ΔE_p]/V
1	0.79 (0.74) [0.42]		−1.73 (1.0) [0.45]
2	0.46 (1.0)[b] [0.21]	0.66[c] [0.27]	−1.80 (1.0) [0.24]
3	0.85 (0.64) [0.22]		−1.07 (1.0) [0.20][d]
5	0.47 (1.0)[b] [0.21]	0.75[c] [0.21]	−1.76 (1.0) [0.24]
6	0.90 (1.0) [0.15]		−1.53 (1.0) [0.14]
7	0.97 (1.0) [0.23]		−1.65 (1.0) [0.24]
8	0.95 (0.59) [0.20]		−1.60 (0.95) [0.21]
9	0.21 (1.0)[b] [0.21]	0.59[c] [0.32]	−1.98 (1.0) [0.26]
10	0.17 (1.0)[b] [0.31]	0.40[c] [0.29]	−2.08 (0.70) [0.36]

[a] All data collected from thf solutions containing 0.1 M $[nBu_4N]PF_6$ as a supporting electrolyte at −30 °C. Scan rate 100 mV s^{-1}, platinum disk working electrode, platinum wire counter and pseudo reference electrodes. Internal ferrocene–ferrocenium reference couple at 0.56 V. E°_{Ox1} = first oxidation potential; E°_{Ox2} = second oxidation potential; E°_{Red1} = first reduction potential; E°_{Red2} = second reduction potential; $i_{pa}:i_{pc}$ = ratio of anodic to cathodic peak current; ΔE_p = peak-to-peak separation. [b] Measured from the isolated wave. [c] Unresolved. [d] Also E°_{Red2} −1.49 (unresolved) [0.47].

In each case the CV response was characterised by a single oxidation and a single reduction process. Compounds **6** and **7**, which feature the cluster bound $SiMe_3$ group, exhibited chemically reversible redox chemistry, while the less sterically hindered **8** displayed less chemically reversible redox behaviour, even at low temperature.

For each of the Ru^{II}-substituted complexes **9** and **10** a single reduction, which was reversible only in the case of the $SiMe_3$ cluster capped complex **9**, was observed. The oxidation sweeps contained two waves, the first of which were shown to be reversible by switching the direction of the voltammetric sweep prior to the onset of the second oxidation. In the case of **9** the second oxidation is complicated by an ECE (electrochemical step–chemical step–electrochemical step) process as evidenced by the ratio of peak currents $i_{pa2} \approx 2i_{pa1}$. The electrochemical data suggest that the ruthenium(II) centres in **9** and **10** result in systems that are more easily oxidised and less easily reduced than **2**, which contains the $C_6H_4NMe_2$-4 group.

Electronic spectra

The visible absorption spectrum of complex **1** exhibited a distinct visible d–d type band near 543 nm. For **2** the presence of the NMe_2 group resulted in a red shift in the lowest energy absorption band (565 nm). In the case of **3** the lowest energy absorption at 552 nm (CH_2Cl_2) displayed significant solvatochromic behaviour [λ_{max} = 543 (cyclohexane), 563 nm (DMF)]. In addition an intense new absorption was observed at 424 nm and is attributed to π–π* transitions associated with the $C_6H_4NO_2$-4 group. A similar effect of smaller magnitude was found for the cyano substituted complex **4** [λ_{max}(cyclohexane) = 540, (DMF) = 550 nm]. Exchange of the organic substituents on the aromatic ring for the organometallic fragment $Cp(PPh_3)_2RuC{\equiv}C$ (**5**) gave a spectrum similar in profile to that of the $C_6H_4NMe_2$-4 substituted cluster, with a smaller absorption coefficient for the visible transitions.

The UV-Vis spectra of complexes **6**–**8** were dominated by the characteristic UV bands below 350 nm associated with π–π* transitions within the phenyl groups of the bisphosphine ligand. The visible region contained broad low intensity absorption bands with λ_{max} between 450 and 500 nm.

Complexes **9** and **10** with the $Cp(PPh_3)_2RuC{\equiv}C$ moiety and $SiMe_3$ or H groups adorning the carbon vertices of the C_2Co_2 core respectively show very similar absorption profiles. The relatively intense absorptions in the visible region (λ_{max} = 600, **9**; 599 nm, **10**) are substantially red shifted in comparison with those found in the spectra of **6**, **7** and **8**. The spectra of **6**–**10** showed virtually no solvatochromic behaviour.

Discussion

Computational work has shown that the visible spectra of $[Co_2(\mu\text{-}RC_2R')(CO)_4(dppm)]$ complexes feature three distinct absorption bands corresponding to excitations from the Co_2C_2 centered HOMO to unoccupied Co_2C_2 based unoccupied orbitals.[17] The position of the visible absorption bands of complexes such as **1**–**10** therefore provides an indication of the degree of orbital reorganisation within the cluster core and hence a measure of the interactions between the various substituents and the cluster core.

The absorption spectra of complexes **1**–**3** exhibited a pronounced red shift in the energy of the visible band and increased absorption coefficient in comparison with those of the ethynyl substituted clusters **6**–**8**. For **2**, the electronic spectral data, together with the electrochemical measurements, indicate that the HOMO for the NMe_2 substituted cluster lies at higher energy than for the simple phenyl cluster **1**. The UV-Vis spectrum of **3**, which features the electron-withdrawing NO_2 group, has a curiously similar λ_{max} value to that of **2**. Given the low potential of the first reduction potential of **3** and comparable oxidation potentials of **1** and **3**, the red shift observed in the spectrum of **3** relative to **1** is attributed to transitions from the HOMO to the relatively low-lying LUMO.

The solvatochromic behaviour of complexes **3** and **4** is consistent with a large change in polarity of the excited state relative the ground state. The other complexes reported in this work feature a more pronounced ground state dipole [$X^{\delta+}$ (or $Ru^{\delta+}$)→$Co_2C_2^{\delta-}$] and negligible solvatochromic behaviour, which is consistent with a more limited change in dipole moment upon excitation. We therefore suggest that the LUMOs of the complexes examined in this study are predominantly centred on the Co_2C_2 cluster core. Cluster centred LUMOs were also found in our earlier study on related (poly)ynyl bridged systems.[17]

The frontier orbital composition of the tetrahedral core common to all the compounds described in this work has extensively been studied by Hoffmann and others.[26] The HOMO was found to present a p-type orbital fragment parallel to the Co–Co vector. A qualitative diagram showing this HOMO interacting with the highest occupied orbital of a phenyl group is illustrated in Fig. 7. The Figure shows that the $C_{p\pi}$ orbital interactions which occur along the C(3)–C(34) bond (as defined in Figs. 1–6) contain both occupied bonding and occupied anti-bonding components. Thus, to a first approximation, C(3)–C(34) should be essentially a single (σ) bond with no net π-bonding contribution. However, the net π-orbital contribution on C(34), and thus the degree to which these π-bonding and π-antibonding components cancel each other out, is sensitive to the electronic nature of the *para* substituent *via* the introduction of mixing effects amongst the benzene-type orbitals.[27] In the most qualitative of terms, electron-withdrawing groups will reduce the π-electron density at C(34), whereas electron-donating groups will increase the π density at the same atom. The corollary to this is that electron-withdrawing groups should increase the net π-bonding interaction along the C(3)–C(34) bond, whereas the presence of electron-donating groups will lead to the opposite behaviour. Thus, for complexes featuring electron-withdrawing groups one might expect a preferential orientation of the phenyl group in a configuration which leads to better π-orbital overlap with the cluster, whereas for electron-donating groups one should expect relatively free rotation around the C(3)–C(34) bond with the lowest energy conformation being dictated largely by steric considerations. We note that similar suggestions have been offered previously to explain the restricted rotation of the phenyl group observed in the alkyne complex $[Co_2(\mu\text{-}\eta^2\text{-}HC_2Ph)(CO)_6]$.[28]

In keeping with this qualitative MO description, the solid state structures of complexes **1** and **2** illustrate a re-orientation

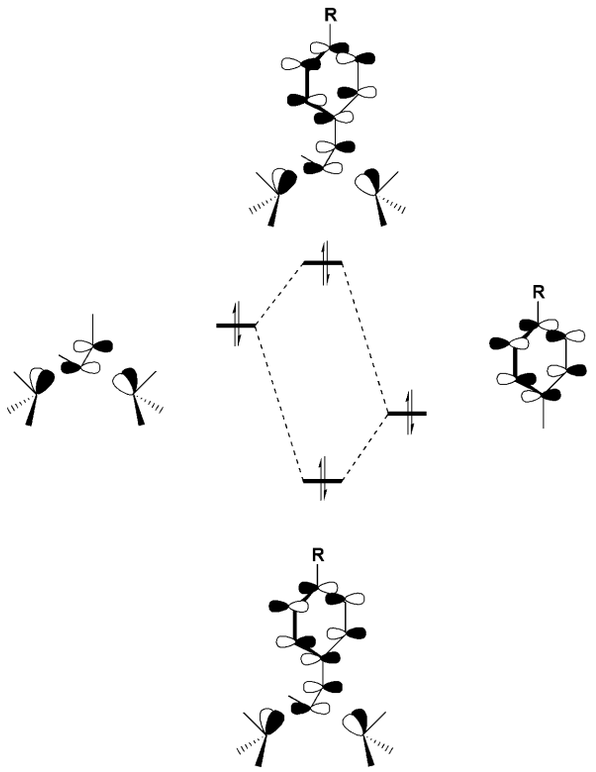

Fig. 7 Pictorial representation of the π-interactions between the Co_2-(alkyne)$(CO)_6$ and aryl fragments.

of the plane of the phenyl ring from that in which orbital overlap would occur and indicates that a limited degree of π character is associated with the C(3)–C(34) bond. Likewise, the introduction of an electron-withdrawing substituent in the *para* position (**3**, **4**) gives complexes in which the phenyl ring is found lying in the crystallographic mirror plane, bisecting the Co–Co bond and co-planar with the C(3)–C(4) vector. Furthermore we note the contraction of the C(34)–C(3) bond in **3** [1.458(3) Å] relative to the other members of the series, and that the C(31)–N separation [1.460(2) Å] is significantly shorter than that found in nitrobenzene [1.492 Å].[29]

Complex **5** may be considered to be a RuC≡CPh fragment fused at the *para* position to a Co_2C_2 tetrahedral core. While it has been established that Ru–C and C≡C bond lengths are relatively insensitive probes of the electronic character of [Ru(C≡CR)$(PR_3)_2$Cp] complexes, the Ru–P bond lengths are more susceptible to minor changes in the electron density of the metal centre.[23,24] The structural information presented above is consistent with a decrease in the electron density at the Ru in **5** relative to that of the simple phenyl acetylide complex [Ru(C≡CPh)$(PPh_3)_2$Cp]. This observation, together with the red shift in the lowest energy absorption band associated with the cobalt fragment and the electrochemical data, clearly indicates that there is a degree of interaction between the mononuclear ruthenium fragment and the cluster core.

The orbital structure of the Cp$(PPh_3)_2$RuC≡CPh fragment has been established, and in the orientation found in the solid state structure of complex **5** the ruthenium dπ component perpendicular to the plane of the ring is able to interact with the HOMO of the phenyl group (Fig. 8).[30] As with the interaction between the phenyl ring and the C_2Co_2 cluster, the $C_{p\pi}$ orbitals along the C(2)–C(31) bond in **5** have both filled bonding and antibonding contributions and thus, to a first approximation, a net π-bond order of zero. However, as before substitution on the benzene ring and the resulting electronic effects can modify the degree to which these components cancel each other and lead to a preferred conformation that allows for a small net bonding π interaction. It is interesting that in the solid state the

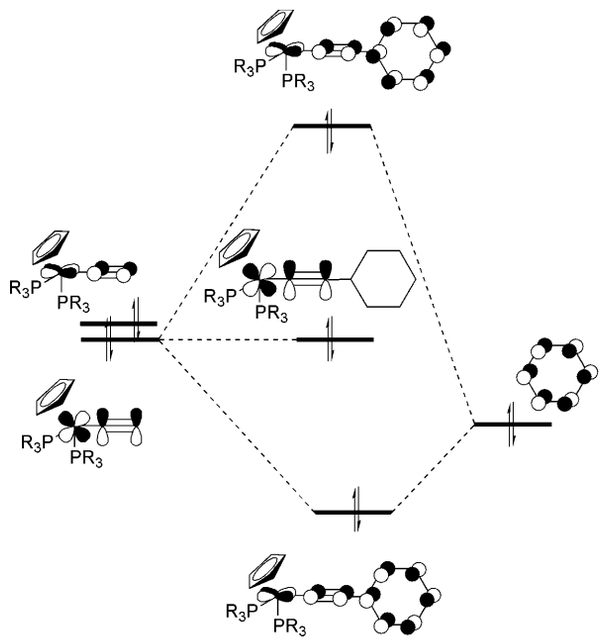

Fig. 8 Interaction diagram for the Cp$(PPh_3)_2$RuC≡C and aryl π systems [adapted from ref. 30].

phenyl acetylide ring of Ru(C≡CPh)$(PPh_3)_2$Cp is disordered over two sites,[24] each conjugated with one of the two ruthenium dπ components.

A qualitative examination of Figs. 7 and 8 suggests that frontier orbital overlap between the Cp$(PPh_3)_2$RuC≡CC_6H_4 and Co_2C_2 moieties will occur optimally when the C_6H_4 plane bisects both the P(3)–Ru–P(4) bond angle and the Co–Co bond. Therefore the geometry of this complex in the solid state (Fig. 5) suggests that while the RuC≡CPh π system is conjugated, conjugation does not extend to the cluster. This proposal is supported by the relevant bond lengths, with **5** featuring a shorter C(2)–C(31) bond [1.432(3) Å] than the simple phenylacetylide complex [Ru(C≡CC_6H_5)$(PPh_3)_2$Cp] [1.456(4) Å][24] and a C(34)–C(3) bond length identical to that found in **1** (Table 2). The lack of an extended conjugation π system is likely the reason that the spectral properties of **6** are not as prominent as those of **9** and **10** (see below).

The electronic structures of the complexes [Co_2(μ-η^2-RC_2-$(C≡C)_n${Ru$(PPh_3)_2$Cp}$(CO)_4$(dppm)] (n = 1, R = C≡CSiMe_3; n = 2, R = SiMe_3) have been described recently.[17] In both cases the HOMO was shown to include significant contributions from the Ru$(PR_3)_2$Cp, $(C≡C)_n$ and the Co_2C_2 cluster core, and as a result is extensively delocalised across the entire molecule. This mixing was shown to destabilise the predominantly Co_2C_2-centred orbital with respect to that of the parent cluster, which accounts for the red-shifted optical spectra when compared with those of simple [Co_2(μ-RC_2R')$(CO)_4$(dppm)] species. Partial charge transfer from the Ru-based electron donor to the cluster-based electron acceptor in the ground state results in an accumulation of negative charge at the Co_2C_2 core and a depletion of charge at the mononuclear terminus, while the charge on the acetylenic bridge remains essentially invariant. The structural and spectroscopic similarity of these complexes to **9** and **10** suggests that an analogous mixing of RuC≡C and Co_2C_2 fragment orbitals is likely to contribute to the HOMO. The similar spectroscopic and electrochemical properties of **9** and **10** suggest that there is little contribution from silicon based orbitals to the frontier orbitals of these molecules.

Conclusion

The spectroscopic, electrochemical and structural features of a series of redox-active complexes featuring a dicobalt alkyne

Table 4 Crystallographic details for complexes **1**–**5**, **9**

	1	**2**	**3**	**4**	**5**	**9**
Formula	$C_{37}H_{28}Co_2O_4P_2$	$C_{39}H_{33}Co_2NO_4P_2$	$C_{37}H_{27}Co_2NO_6P_2$	$C_{38}H_{27}Co_2NO_4P_4$	$C_{83}H_{70}Co_2O_4P_4RuSi{\cdot}CH_2Cl_2$	$C_{77}H_{66}Co_2O_4P_4RuSi$
M	716.39	759.46	761.40	741.41	1587.22	1426.20
Crystal system	Monoclinic	Monoclinic	Orthorhombic	Monoclinic	Monoclinic	Orthorhombic
Space group	*C*2/*c*	$P2_1/c$	*Pbcm*	$P2_1/m$	$P2_1/n$	$P2_12_12_1$
a/Å	39.6115(10)	14.301(10)	14.4825(11)	9.3295(2)	19.4088(9)	13.7464(5)
b/Å	12.2498(3)	15.716(10)	13.6742(10)	16.6546(4)	19.2738(9)	19.9035(6)
c/Å	14.6345(4)	15.727(10)	16.8860(14)	11.1253(3)	20.0688(10)	24.8998(8)
β/°	92.074(2)	98.792(2)	90	92.212(1)	97.390(1)	90
U/Å^3	7096.9(3)	3493.2(4)	3344.0(4)	1727.35(7)	7445.0(6)	6812.6(4)
T/K	100(2)	100(2)	100(2)	100(2)	100(2)	100(2)
Z	8	4	4	2	6	4
μ/mm^{-1}	1.061	1.083	1.136	1.093	1.298	0.861
Reflections measured, unique (R_{int})	38965, 9374 (0.0269)	35790, 8011 (0.0585)	39675, 4608 (0.1189)	21205, 4731 (0.0293)	58747, 19733 (0.0374)	86568, 18038 (0.0452)
$wR(F^2)$ (all data)	0.0793	0.0820	0.0794	0.0676	0.1133	0.0635

cluster core and a phenyl-based spacing unit have been rationalised using a qualitative MO argument. The phenyl bridge permits a degree of π conjugation only when strongly electron-withdrawing groups are placed *para* to the redox-active cluster probe group. In the absence of a π-conjugation pathway, electronic interactions with the cluster probe group must be more electrostatic in origin. In combination with the particular organometallic fragments examined in this work, the inherent stability of the phenyl ring π system does not favor the formation of compounds in which orbitals extend over the entire molecule. This is in direct contrast to the situation found for pure ynyl bridges.

Experimental

General conditions

All reactions were carried out under dry high-purity nitrogen using standard Schlenk techniques. Solvents were dried and distilled with the exception of AnalR methanol, prior to use. Preparative TLC was performed on 20 × 20 cm glass plates coated with silica gel (Merck GF_{254}, 0.5 mm thick). Literature methods were used to prepare the alkynes $HC{\equiv}CC_6H_4X$,[31] $[Co_2(CO)_6(dppm)]$,[32] $[Co_2(\mu\text{-}\eta^2\text{-}RC_2C{\equiv}CR')(CO)_4(\mu\text{-dppm})]$ **6**, **7**, **8**[33] and $[Ru(C{\equiv}CC_6H_4C{\equiv}CSiMe_3)(PPh_3)_2Cp]$.[25] Other reagents were purchased and used as received.

Instrumental measurements

Infrared spectra were recorded using calcium fluoride cells of 0.5 mm path length on a Perkin-Elmer 1600 Series FT-IR spectrometer, UV-Vis spectra from CH_2Cl_2 solutions in a 1 cm path length quartz cuvette on a Varian Cary 5 UV-Vis-NIR spectrometer and NMR spectra with a Varian VXR-400s at (^{1}H) 399.97 MHz and (^{13}C) 100.57 MHz in $CDCl_3$ and referenced against the solvent resonances. ES MS spectra were obtained using a Fisons instrument with a cone voltage of 30 V. Solutions of compounds in CH_2Cl_2 in MeOH were introduced *via* an induction loop with sodium methoxide solution added *in situ* as an aid to ionisation. Cyclic voltammetry experiments were recorded using an EG&G Versastat II instrument in thf containing 0.1 M $[NBu_4]PF_6$. Solutions were purged with nitrogen and measured with a platinum working electrode with platinum wire reference and counter electrodes at low temperature such that the ferrocene–ferrocenium redox couple was located at 0.56 V. Microanalyses were performed in house.

Preparations

$[Co_2(\mu\text{-}\eta^2\text{-}HC_2C_6H_4X\text{-}4)(CO)_4(\mu\text{-dppm})]$ (X = H, 1; NMe_2, 2; NO_2, 3 or CN, 4). A solution of $[Co_2(CO)_4(dppm)]$ (200 mg, 0.30 mmol) and $HC{\equiv}CC_6H_4X$ (0.30 mmol) in benzene (15 ml) was heated at reflux for 1 h. The solvent was removed and the residue purified by preparative TLC (30% acetone in hexane) to give a single band, which was crystallised (CH_2Cl_2–MeOH) to afford large crystals of the desired product.

$[Co_2(\mu\text{-}\eta^2\text{-}Me_3SiC_2C_6H_4C{\equiv}C\{Ru(PPh_3)_2Cp\})(CO)_4(\mu\text{-dppm})]$ 5. A solution of $[Co_2(CO)_6(dppm)]$ (100 mg, 0.15 mmol) and $[Ru(C{\equiv}CC_6H_4C{\equiv}CSiMe_3)(PPh_3)Cp]$ (133 mg, 0.15 mmol) in benzene (12 ml) was heated at reflux. The bright yellow-orange solution darkened slowly to give a brown solution and after 1.5 h TLC analysis indicated only one brown product. The solvent was removed and the residue purified by preparative TLC (30% acetone in hexane). The sole brown band yielded complex **5** as tan coloured crystals (CH_2Cl_2–MeOH) suitable for X-ray study.

$[Co_2(\mu\text{-}\eta^2\text{-}Me_3SiC_2C{\equiv}C\{Ru(PPh_3)_2Cp\})(CO)_4(\mu\text{-dppm})]$ 9. A solution of $[RuCl(PPh_3)_2Cp]$ (100 mg, 0.14 mmol) and complex **2** (101 mg, 0.14 mmol) in MeOH (15 ml) was treated with NH_4PF_6 (22 mg, 0.14 mmol) and heated at reflux for 1 h. Note: thf (0.5 ml) may be added to aid solvation of the starting materials if poorly solvated after some 15 minutes of reflux. During this time the orange-red solution turned dark green and a similarly coloured precipitate was observed. The solution was allowed to cool and treated with NaOMe solution. Filtration gave the crude dark green product **9**. Recrystallisation from CH_2Cl_2–EtOH (slow evaporation) gave crystals suitable for X-ray study.

$[Co_2\{\mu\text{-}\eta^2\text{-}HC_2C{\equiv}C\{Ru(PPh_3)_2Cp\}\})(CO)_4(\mu\text{-dppm})]$ 10. A solution of $[RuCl(PPh_3)_2Cp]$ (100 mg, 0.14 mmol) and complex **3** (93 mg, 0.14 mmol) in MeOH (15 ml) was treated with NH_4PF_6 (22 mg, 0.14 mmol). The mixture was refluxed for 3 h, by which time it had darkened, the orange $[RuCl(PPh_3)_2Cp]$ had been consumed and a dark green precipitate was evident. Treating the cooled solution with NaOMe gave further green precipitate which was filtered off affording crude **10** which was recrystallised from CH_2Cl_2–EtOH (slow evaporation).

Crystallography

Data were collected on a Bruker SMART CCD diffractometer, using graphite-monochromated Mo-Kα radiation ($\lambda = 0.71073$ Å). The structures were solved by direct methods and refined by full-matrix least squares against F^2 on all data, using the SHELXTL suite of programs.[34] All phenyl group hydrogen atoms were placed in calculated positions and refined using a riding model. Crystallographic data are collected in Table 4.

The structure of complex **1** contained disordered solvent of crystallisation (CH_2Cl_2/methanol). This residual electron density was treated successfully with the utility "Squeeze" available in the crystallographic suite PLATON.[35] Prior to treatment, the volume of the solvent accessible void as reported

by the Squeeze routine was 816.8 Å^3 and the residual electron count per cell was 235. The refinement with all the electron density in the solvent void intact (*i.e.* left as Q-peaks) gave a $R1$ value of 0.0699 and $Rw2$ value of 0.2176.

CCDC reference number 186/2280.

See http://www.rsc.org/suppdata/dt/b0/b008445j/ for crystallographic files in .cif format.

Acknowledgements

This work was supported by the Department of Chemistry, Durham University. We gratefully acknowledge a generous gift of the substituted acetylenes used in this study by Professor T. B. Marder and Dr R. L. Thomas.

References

1 D. Astruc, *Acc. Chem. Res.*, 1997, **30**, 383.
2 R. Schennach, D. G. Naugle, D. Cocke, R. Dembinski and J. A. Gladysz, *Vacuum*, 2000, **56**, 115.
3 F. Paul and C. Lapinte, *Coord. Chem. Rev.*, 1998, **178**–**180**, 431.
4 J.-P. Launay and C. Coudret, in *Electron Transfer in Chemistry*, eds. V. Balzani and A. P. de Silva, Wiley-VCH, New York, 2000, vol. 5.
5 Y. Wada, M. Tsukada, M. Fujihira, K. Matsushige, T. Ogawa, M. Haga and S. Tanaka, *Jpn. J. Appl. Phys.*, 2000, **39**, 3835.
6 N. Le Narvor, L. Toupet and C. Lapinte, *J. Am. Chem. Soc.*, 1995, **117**, 7129.
7 R. Dembinski, T. Bartik, B. Bartik, M. Jaeger and J. A. Gladysz, *J. Am. Chem. Soc.*, 2000, **122**, 810.
8 M. I. Bruce, P. J. Low, K. Costuas, J.-F. Halet, S. P. Best and G. A. Heath, *J. Am. Chem. Soc.*, 2000, **122**, 1949.
9 S. Kheradmandan, K. Hainze, H. W. Schmalle and H. Berke, *Angew. Chem., Int. Ed.*, 1999, **38**, 2270.
10 G. H. Worth, B. H. Robinson and J. Simpson, *Organometallics*, 1992, **11**, 3863.
11 D. Osella, O. Bambino, C. Nervi, M. Ravera and D. Bertolino, *Inorg. Chim. Acta*, 1993, **206**, 155.
12 M. I. Bruce, J.-F. Halet, S. Kahal, P. J. Low, B. W. Skelton and A. H. White, *J. Organomet. Chem.*, 1999, **578**, 155.
13 F. Coat, M.-A. Guillevic, L. Toupet, F. Paul and C. Lapinte, *Organometallics*, 1997, **16**, 5988.
14 F. Paul, W. E. Meyer, L. Toupet, H. J. Jiao, J. A. Gladysz and C. Lapinte, *J. Am. Chem. Soc.*, 2000, **122**, 9405.
15 Y. B. Zhu, O. Clot, M. O. Wolf and G. P. A. Yap, *J. Am. Chem. Soc.*, 1998, **120**, 1812.
16 M. C. B. Colbert, J. Lewis, N. J. Long, P. R. Raithby, A. J. P. White and D. J. Williams, *J. Chem. Soc., Dalton Trans.*, 1997, 99.
17 P. J. Low, R. Rousseau, P. Lam, K. A. Udachin, G. D. Enright, J. S. Tse, D. D. M. Wayner and A. J. Carty, *Organometallics*, 1999, **18**, 3885.
18 R. S. Dickson and P. J. Fraser, *Adv. Organomet. Chem.*, 1974, **12**, 323.
19 W. Henderson, B. K. Nicholson and L. J. McCaffrey, *Polyhedron*, 1998, **17**, 4291.
20 J. Manna, K. D. John and M. D. Hopkins, *Adv. Organomet. Chem.*, 1995, **38**, 79.
21 D. L. Thorn and R. Hoffmann, *Inorg. Chem.*, 1978, **17**, 126.
22 R. P. Aggarwal, N. G. Connelly, M. C. Crespo, B. J. Dunne, P. M. Hopkins and A. G. Orpen, *J. Chem. Soc., Dalton Trans.*, 1992, 655.
23 I. R. Whittal, M. G. Humphrey, D. C. R. Hockless, B. W. Skelton and A. H. White, *Organometallics*, 1995, **14**, 3970.
24 J. M. Wisner, T. J. Basrtczak and J. A. Ibers, *Inorg. Chim. Acta*, 1985, **100**, 115.
25 M. I. Bruce, B. C. Hall, B. D. Kelly, P. J. Low, B. W. Skelton and A. H. White, *J. Chem. Soc., Dalton Trans.*, 1999, 3719.
26 D. M. Hoffmann, R. Hoffmann and C. R. Fisel, *J. Am. Chem. Soc.*, 1982, **104**, 3858.
27 T. A. Albright, J. K. Burdett and M.-H. Whangbo, *Orbital Interactions in Chemistry*, John Wiley and Sons, New York, 1985, ch. 3.
28 P. Yuan, M.-J. Don, M. G. Richmond and M. Schwartz, *Inorg. Chem.*, 1992, **31**, 3491.
29 E. M. Graham, V. M. Miskowski, J. W. Perry, D. R. Coulter, A. E. Steigman, W. P. Schaefer and R. E. Marsh, *J. Am. Chem. Soc.*, 1989, **111**, 8771.
30 J. E. McGrady, T. Lovell, R. Stranger and M. G. Humphrey, *Organometallics*, 1997, **16**, 4004.
31 P. Mguyen, Z. Yuan, L. Agcos, G. Lesley and T. B. Marder, *Inorg. Chim. Acta*, 1994, **220**, 289.
32 L. S. Chia and W. R. Cullen, *Inorg. Chem.*, 1975, **14**, 482.
33 M. I. Bruce, P. J. Low, A. Werth, B. W. Skelton and A. H. White, *J. Chem. Soc., Dalton Trans.*, 1996, 1551.
34 G. M. Sheldrick, SHELXTL PC, version 5.03, Siemens Analytical Instrumentation, Madison, WI, 1994.
35 A. L. Spek, *Acta Crystallogr., Sect. A*, 1990, **46**, C34.